# SENSING ANOMALIES AS POTENTIAL HAZARDS: DATASETS AND BENCHMARKS

Dario Mantegazza, Carlos Redondo, Fran Espada, Luca M. Gambardella, Alessandro Giusti and Jérôme Guzzi \*

October 29, 2021

# **ABSTRACT**

We consider the problem of detecting, in the visual sensing data stream of an autonomous mobile robot, semantic patterns that are unusual (i.e., anomalous) with respect to the robot's previous experience in similar environments. These anomalies might indicate unforeseen hazards and, in scenarios where failure is costly, can be used to trigger an avoidance behavior. We contribute three novel image-based datasets acquired in robot exploration scenarios, comprising a total of more than 200k labeled frames, spanning various types of anomalies. On these datasets, we study the performance of an anomaly detection approach based on autoencoders operating at different scales.

# **Supplementary Material**

Videos, code, and data available at https://github.com/idsia-robotics/hazard-detection.

## 1 Introduction

Many emerging applications involve a robot operating autonomously in an unknown environment; the environment may include hazards, i.e., locations that might disrupt the robot operation, possibly causing it to crash, get stuck, and more generally to fail its mission. Robots are usually capable to perceive hazards that are expected during system development and therefore can be explicitly accounted for when designing the perception subsystem. For example, ground robots can typically perceive and avoid obstacles or uneven ground.

In this paper, we study how to provide robots with a different capability: detecting *unexpected* hazards, potentially very rare, that were not explicitly considered during system design. Because we don't have any model of how these hazards appear, we consider anything that is novel or unusual as a potential hazard to be avoided.

Animals and humans exhibit this exact behavior [1], known as *neophobia* [2]: "the avoidance of an object or other aspect of the environment solely because it has never been experienced and is dissimilar from what has been experienced in the individual's past" [3]. We argue that autonomous robots could benefit from implementing neophobia, in particular whenever the potential failure bears a much higher cost than the avoidance behavior. Thus, for example, for a ground robot it makes sense to avoid unusual-looking ground [4] when a slightly longer path on familiar ground is available; or a planetary rover might immediately stop a planned trajectory if something looks odd, waiting for further instructions from ground control after operators review the unusual data.

Our experiments are motivated by a similar real-world use case in which a quadrotor equipped with sophisticated sensing and control traverses underground tunnels for inspection of aqueduct systems. During the flights, that might span several kilometers, the robot is fully autonomous since it has no connectivity to the operators; they wait for the robot to either reach the predetermined exit point, or — in case the robot decides to abort the mission — backtrack to the entry. In this context, a crash bears the cost of the lost hardware and human effort, but most importantly of the lost

<sup>\*</sup>Dario Mantegazza, Luca M. Gambardella, Alessandro Giusti, and Jérôme Guzzi are with the Dalle Molle Institute for Artificial Intelligence (IDSIA), USI-SUPSI, Lugano, Switzerland. Carlos Redondo and Fran Espada are with Hovering Solutions Ltd, Madrid, Spain. This work is supported by the Swiss National Science Foundation (SNSF) through the NCCR Robotics and by the European Commission through the Horizon 2020 project 1-SWARM, grant ID 871743.

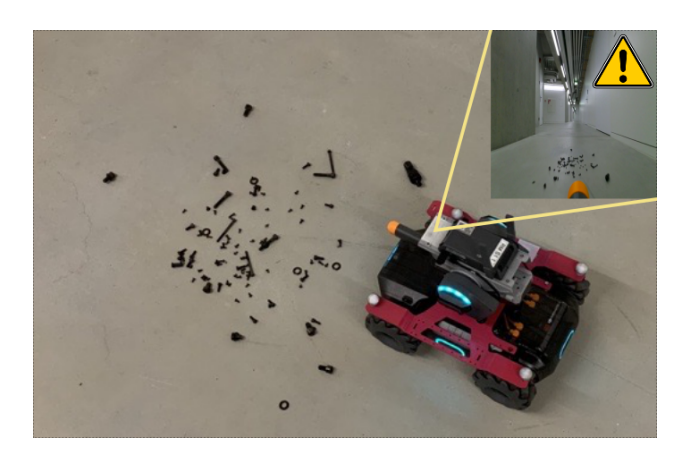


Figure 1: A Robomaster detects an anomaly in the camera frame: cautiousness is required.

information concerning the hazard that determined the failure, that remains unknown. It then makes sense to react to unexpected sensing data by aborting the mission early and returning to the entry point;<sup>2</sup> operators can then analyze the reported anomaly: in case it is not a genuine hazard, the system can be instructed to ignore it in the current and future missions, and restart the exploration.

After reviewing related work (Section 2), we introduce in Section 3 our **main contribution**: three image-based datasets (one simulated, two real-world) from indoor environment exploration tasks using ground or flying robots; each dataset is split in training (only normal frames) and testing sets; testing frames are labeled as normal or anomalous, representing hazards that are meaningful in the considered scenarios, including sensing issues and localized or global environmental hazards. In Section 4, we describe an anomaly detection approach based on autoencoders and in Section 5 we report and discuss extensive experimental results on these datasets, specifically exploring the impact of image sampling and pre-processing strategies on the ability to detect hazards at different scales.

# 2 Related Work

## 2.1 Anomaly detection methods

Anomaly Detection (AD) is a widely-researched topic in Machine Learning; general definitions of anomalies are necessarily vague: e.g., "an observation that deviates considerably from some concept of normality" [6], or "patterns in data that do not conform to expected behavior" [7]. When operating on high-dimensional inputs, such as images, the problem often consists in finding *high-level* anomalies [6] that pertain the data semantics, and therefore imply some level of understanding of the inputs. Methods based on deep learning have been successful in high-level anomaly detection in various fields, including medical imaging [8], industrial manufacturing [9, 10], surveillance [11], robot navigation [4], fault detection [12], intrusion detection [13] and agriculture [14].

A widespread class of approaches for anomaly detection on images, which we adopt in this paper as a benchmark, is based on undercomplete autoencoders [15]: neural models that take the image as input and are trained to reproduce it as their output (e.g., using a Mean Absolute Error loss), while constraining the number of nodes in one of the hidden layers (the *bottleneck*); this limits the amount of information that can flow through the network, and prevents the autoencoder from learning to simply copy the input to the output. To minimize the loss on a large dataset of normal (i.e., non-anomalous) samples, the model has to learn to compress the inputs to a low-dimensional representation that captures their high-level information content. When tasked to encode and decode an anomalous sample, i.e., a sample from a different distribution than the training set, one expects that the model will be unable to reconstruct it correctly. Measuring the reconstruction error for a sample therefore yields an indication of the sample's anomaly. Variational Autoencoders [16] and Generative Adversarial Networks (GAN) [17] can also be used for Anomaly Detection tasks, by training them to map vectors sampled from a predefined distribution (i.e., Gaussian or uniform) to the distribution of normal training samples. Flow-based generative models [18] explicitly learn the probability density function of the input data using Normalizing Flows [19].

<sup>&</sup>lt;sup>2</sup>Similarly, retention of information following encounters with novel predators is one of the recognized evolutionary advantages of neophobic animals [5].

One-Class Classifiers, such as Deep SVDD [20] and deep OC-SVM [21], can also be used as anomaly detectors; these methods define a decision boundary around the training instances in their respective latent spaces.

# 2.2 Anomaly detection on images

In recent work, Sabokrou et al. [22] propose a new adversarial approach using an autoencoder as a reconstructor, feeding a standard CNN classifier as a discriminator, trained adversarially. During inference, the reconstructor is expected to enhance the inlier samples while distorting the outliers; the discriminator's output is used to indicate anomalies.

Sarafijanovic introduces [23] an Inception-like autoencoder for the task of anomaly detection on images. The proposed method uses different convolution layers with different filter sizes all at the same level, mimicking the Inception approach [24]. The proposed model works in two phases; first it trains the autoencoder only on normal images, then, instead of the autoencoder reproduction error, it measure the distance over the pooled bottleneck's output, which keeps the memory and computation needs at a minimum. The authors test their solution over some classical computer vision datasets: MNIST [25], Fashion MNIST [26], CIFAR10 and CIFAR100 [27].

# 2.3 Application to robotics

On low-dimensional time-series data A large amount of literature deals with detecting anomalies using low-dimensional (but potentially high-frequency) data streams from proprioceptive or exteroceptive sensors. On this type of data, Khalastchi et al. rely on simple metrics such as the Mahalanobis Distance with good results in multiple scenarios [28, 12], whereas Sakurada et al. [29] compare autoencoders to PCA and kPCA for spacecraft telemetry data. Birnbaum [13] proposes an approach for detecting cyber attacks, sensors faults or structural failures on Unmanned Aerial Vehicle (UAV) flight data; the approach is based on comparing hand-crafted descriptors of UAV behavior (including state, flight plan and sensor readings) to predefined behavioral profiles. Park et al. tackle anomaly detection in robot assisted feeding, using Hidden Markov Models with hand-crafted features [30], or a combination of Variational Autoencoders and LSTM networks [31]; the latter approach encodes a sequence of multi-modal sensory signals into a latent space, then estimates the expected distribution of the received inputs: an anomaly is detected when the negative log-likelyhood of the current input, given an expected distribution, exceeds a certain threshold.

On high-dimensional data Semantic anomaly detection on high-dimensional sensing data is used in many different robotics application domains. Early attempts concerned with autonomous patrolling [11] apply image matching algorithms between observed data and large databases of normal images, to identify unexpected differences. Christiansen et al. [14], detect obstacles and anomalies on an autonomous agricultural robot, using DeepAnomaly, a custom CNN derived from AlexNet [32]; anomalies are found and highlighted using background subtraction over high-level features of the CNN. Wellhausen et el. [4] achieve safe navigation for a legged ANYmal [33] robot in unknown environments, avoiding footholds located on terrain whose appearance is anomalous with respect to the robot's previous experience; the paper compares a standard autoencoder with two additional models sharing the same encoder: Deep SVDD [20] and Real NVP [18]; Real NVP performed best, followed closely by the autoencoder.

#### 3 Datasets

We contribute three datasets representing different operating scenarios for indoor robots (flying or ground). Each dataset is composed by a large number of grayscale or RGB frames with a  $512 \times 512$  px resolution. For each dataset, we define four subsets:

- a training set, composed by only normal frames;
- a validation set, composed by only normal frames;
- a labeled testing set, composed by frames with an associated label; some frames in the testing set are normal, others are anomalies and are associated with the respective anomaly class;
- an unlabeled qualitative testing set, consisting in one or more continuous data sequences acquired at approximately 30 Hz, depicting the traversal of environments with alternating normal and anomalous situations.

The training set is used for training anomaly detection models, and the validation set for performing model-selection of reconstruction-based approaches – e.g., determining when to stop training an autoencoder. The testing set can be used to compute quantitative performance metrics for the anomaly detection problem. The qualitative testing set can

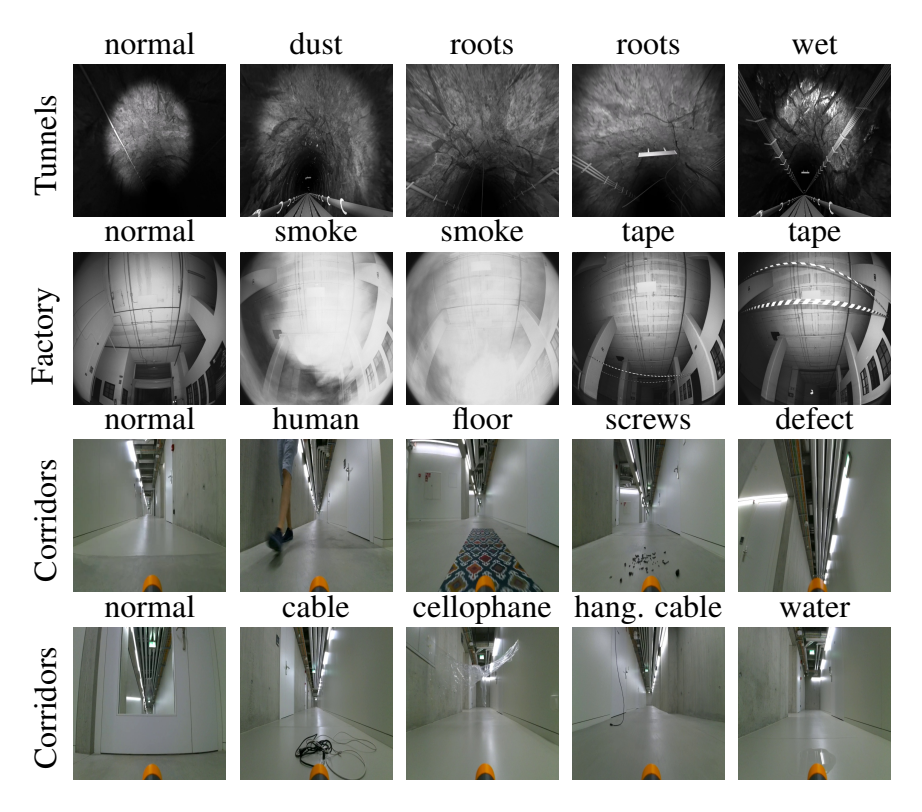


Figure 2: The testing datasets are composed by normal images and by images of different anomaly classes.

be used to analyze how the model, the autoencoder in our case, outputs react to a video stream as the robot traverses normal and anomalous environments.

The very concept of anomaly in robotic perception is highly subjective and application-dependent [13, 14, 4]. Whether a given situation should be considered an anomaly depends on the features of the robot and on its task; for example, consider a robot patrolling corridors with floors normally clear of objects; the presence of screws and bolts littering the ground could be hazardous for a robot with inflated tyres that could get punctured, but completely irrelevant for a drone or legged robot. On an orthogonal dimension, some applications might be interested in determining anomalies regardless on whether they pose an hazard to the robot: in a scenario in which a robot is patrolling normally-empty tunnels, finding anything different in the environment could be a sign of an intrusion and should be detected. The appearance of anomalies in forward-looking camera streams is also dependent on the distance from the robot; wires or other thin objects that might pose a danger to a robot could be simply invisible if they are not very close to the camera. Our labeled testing sets are manually curated, and we used our best judgment to determine whether to consider a frame anomalous or not: frames with anomalies that are not clearly visible in the  $512 \times 512$  full-resolution images are excluded from the quantitative testing set, but they are preserved in the qualitative testing sequences.

#### 3.1 Tunnels dataset

The dataset, provided by Hovering Solutions Ltd, is composed of grayscale frames from simulated drone flights along procedurally-generated underground tunnels presenting features typically found in aqueduct systems, namely: random dimensions; random curvature radius; different structures on the floor; tubing, wiring and other facilities attached to the tunnel walls at random positions; uneven textured walls; various ceiling-mounted features at regular intervals (lighting fixtures, signage). The drone flies approximately along the centerline of the tunnel and illuminates the tunnel walls with a spotlight approximately coaxial with the camera. Both the camera and the spotlight are slightly tilted upwards.

This dataset is composed of 143070 frames: 72854 in the training set; 8934 in the validation set; 57081 in the quantitative labeled testing set (40% anomalous); 4201 in the qualitative testing sequences.

Three anomalies are represented: dust, wet ceilings and thin plant roots hanging from the ceilings (see Figure 2). These all correspond to hazards for quadrotors flying real-world missions in aqueduct systems: excessive amounts of dust raised by rotor downwash hinder visual state estimation; wet ceilings, caused by condensation on cold walls in

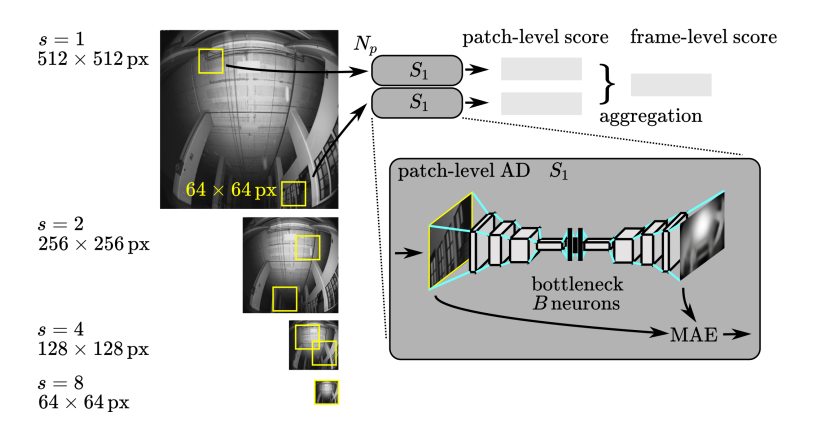


Figure 3: Anomaly detection model: using an autoencoder to compute the patch-level anomaly scores, which are aggregated in a frame-level score.

humid environments, indicates the risk of drops of water falling on the robot; thin hanging roots, which find their way through small cracks in the ceiling, directly cause crashes.

## 3.2 Factory dataset

This dataset contains grayscale frames recorded by a real drone, with a similar setup to the one simulated in the Tunnels dataset, flown in a testing facility (a factory environment) at Hovering Solutions Ltd. During acquisition, the environment is almost exclusively lit by the onboard spotlight.

This dataset is composed of 12040 frames: 4816 in the training set; 670 in the validation set; 6001 in the quantitative testing set (53% anomalous); 553 in the qualitative testing sequences.

Two anomalies are represented: smoke in the environment, generated with a fog machine; and a signaling tape stretched between two opposing walls (Figure 2). These anomalies represent large-scale and small-scale anomalies, respectively.

## 3.3 Corridors dataset

This dataset contains RGB frames recorded by a real teleoperated omni-directional ground robot (DJI Robomaster S1), equipped with a forward-looking camera mounted at  $22.5\,\mathrm{cm}$  from the ground, as it explores corridors of the underground service floor of a large university building; the corridors have a mostly uniform, partially reflective floor with few features; various side openings of different size (doors, lifts, other connecting corridors); variable features on the ceiling, including service ducts, wiring and various configurations of lighting. The robot is remotely teleoperated during data collection, traveling approximately along the center of the corridor.

This dataset is composed of 52607 frames: 25844 in the training set; 2040 in the validation set; 17971 in the testing set (45% anomalous); 6752 in qualitative testing sequences.

8 anomalies are represented, ranging from subtle characteristics of the environment affecting a minimal part of the input, to large-scale changes in the whole image acquired by the robot: water puddles, cables on the floor; hanging cables from the ceiling; different mats on the floor, human presence, screws and bolts on the ground; camera defects (uneven elevation, dirty lens). Examples of these anomalies are in Figure 2.

# 4 Experimental setup

#### 4.1 Anomaly detection on frames

We define an anomaly detector as a function mapping a frame  $(512 \times 512)$  to an anomaly score, which should be high for anomalous frames and low for normal ones. The frame-level anomaly detector relies on a patch-level anomaly detector (see Figure 3), which instead operates on low-resolution inputs  $(64 \times 64)$ , which is a typical input size for anomaly detection methods operating on images [4, 34].

Table 1: AUC values for models at all scales

scale	Avg		Tun	nels		Factory				Corridors							
	all	all	dust	root	wet	all	smoke	tape	all	water	cellophane	cable	defect	hang. cable	floor	human	screws
$S_8$	0.82	0.82	0.54	0.76	0.87	0.90	0.95	0.48	0.74	0.63	0.66	0.70	1.00	0.44	0.85	0.67	0.48
$S_4$	0.62	0.89	0.62	0.79	0.94	0.24	0.25	0.17	0.73	0.81	0.70	0.81	1.00	0.41	0.38	0.73	0.30
$S_2$	0.60	0.88	0.63	0.80	0.93	0.21	0.20	0.30	0.71	0.78	0.70	0.75	0.99	0.50	0.51	0.56	0.40
$S_1$	0.55	0.85	0.61	0.80	0.88	0.12	0.10	0.25	0.69	0.72	0.73	0.68	0.90	0.60	0.59	0.51	0.55

First, the frame is downsampled (using local averaging) by a factor  $s \in \{1, 2, 4, 8\}$ ; we will refer to the respective models as  $S_1$ ,  $S_2$ ,  $S_4$  and  $S_8$ . The resulting downsampled image, with resolution  $512/s \times 512/s$ , is standardized to zero mean and unit variance, independently for each channel; we then extract  $N_p$   $64 \times 64$  patches, at random coordinates, such that they are fully contained in the downsampled image. The patch-level anomaly detector is applied to each patch, producing  $N_p$  anomaly scores; these are aggregated together (e.g., computing their average) to yield the frame-level anomaly score.

Note that in case of  $S_8$ ,  $N_p \equiv 1$  since a unique patch can be defined on a  $64 \times 64$  downsampled image. This corresponds to the special case in which the whole frame (after downsampling) is directly used as input to the patch-based detector. This approach is simple and attractive, but is necessarily limited on small-scale anomalies since it can not leverage the full resolution of the frame.

## 4.2 Patch-level anomaly detector

#### 4.3 Training

For a given scale s, the autoencoder is trained as follows: first, we downsample each frame in the training set by a factor s; then, as an online data generation step, we sample random patches completely contained in the downsampled frames.

We use the Adam [35] optimizer to minimize the mean squared reconstruction error, with an initial learning rate of 0.001, that is reduced by a factor of 10 in case the validation loss plateaus for more than 8 epochs. Because the size of the training set of different datasets is widely variable, we set the total number of epochs in such a way that during the whole training, the model sees a total of 2 million samples; this allows us to better compare results on different datasets.

The approach is implemented in PyTorch and Python 3.8, using a deep learning workstation equipped with 4 NVIDIA 2080 Ti GPUs; training each model takes about 1 h.

# 4.4 Metrics

We evaluate the performance of the frame-level anomaly detector on the testing set of each dataset. In particular, we quantify the anomaly detection performance as if it was a binary classification problem (normal vs anomalous), where the probability assigned to the anomalous class corresponds to the anomaly score returned by the detector. This allows us to define the Area Under the ROC Curve metric (AUC); an ideal anomaly detector returns anomaly scores such that there exists a threshold t for which all anomalous frames have scores higher than t, whereas all normal frames have scores lower than t: this corresponds to an AUC of 1. An anomaly detector returning a random score for each instance, or the same score for all instances, both yield an AUC of 0.5. The AUC value can be interpreted as the probability that a random anomalous frame is assigned an anomaly score larger than that of a random normal frame. The AUC value is a meaningful measure of a model's performance and does not depend on the choice of threshold.

For each model and dataset, we compute the AUC value conflating all anomalies, as well as the AUC individually for each anomaly (versus normal frames, ignoring all other anomalies).

# 5 Results

# 5.1 $S_8$ model hyperparameters

Figure 4 explores the choice of the bottleneck size B for model  $S_8$ . Increasing B reduces reconstruction error for both anomalous and normal data; the reconstruction error best discriminates the two classes (higher AUC, higher average gap between the two classes) for intermediate values of B (16 neurons): then, the autoencoder can reconstruct well normal data while lacking capacity to properly reconstruct anomalous samples. These findings apply to all three datasets. Figure 5 investigates a similar capacity trade-off: autoencoders with a small number of filters for the first convolution layer (first layer size) are not powerful enough to reproduce well even normal samples, therefore have lower discriminating performance. For the rest of the Section, we only report results for bottleneck size B=16 and first layer size F=128.

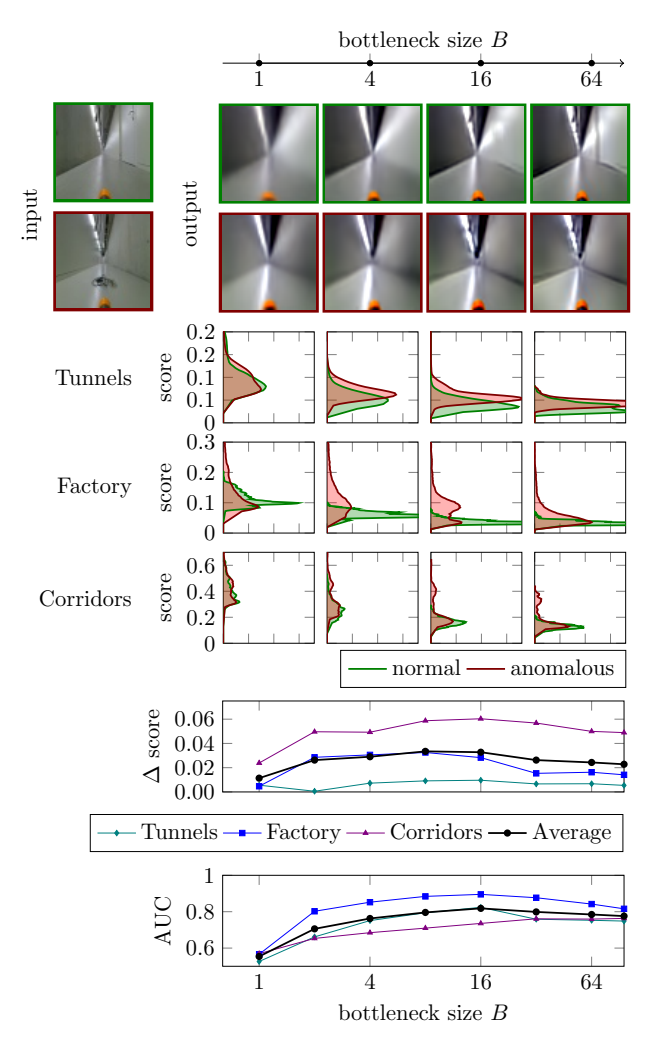


Figure 4: Results for different autoencoder's bottleneck sizes for model  $S_8$ . Top two rows: for the same two samples (normal in green, anomalous in red), autoencoder reconstructions. Center: score distributions over the testing set. Bottom: mean score difference between anomalous and normal samples and AUC of the anomaly detector.

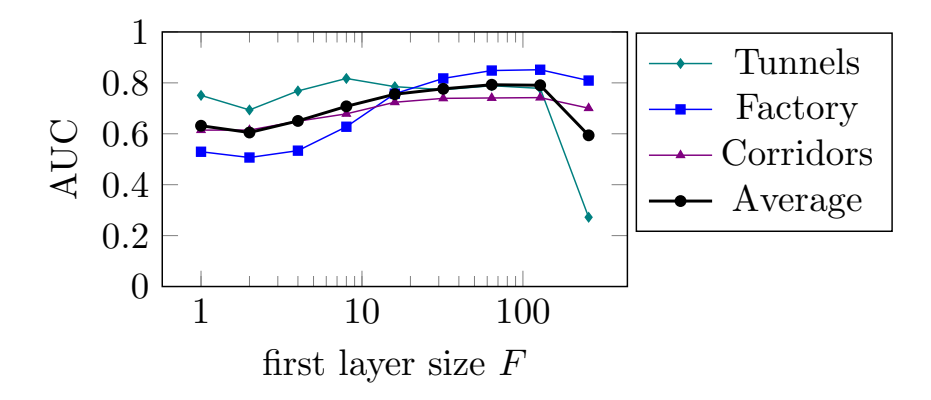


Figure 5: Results for model  $S_8$  for autoencoders with different first layer sizes.

# 5.2 Patch aggregation

Figure 6:left explores the impact of  $N_p$  on the anomaly detection performance of model  $S_2$ ; we observe that, for the Tunnels and Corridors datasets, the performance increases as  $N_p$  increases. This is expected, as more patches are processed and aggregated to compute the frame-level score. Only for Tunnels,  $S_2$  outperforms  $S_8$  for 10 or more patches.

On the contrary, for the Factory dataset the model  $S_2$  performs worse than chance at detecting anomalies, and assigns lower scores than normal data. this is due to the testing set being dominated by the smoke anomaly, which is not detectable at low scales as discussed in Section 5.3.

Figure 6:right reports how computing the 0.7-0.8 quantile offers a slightly better aggregation than averaging.

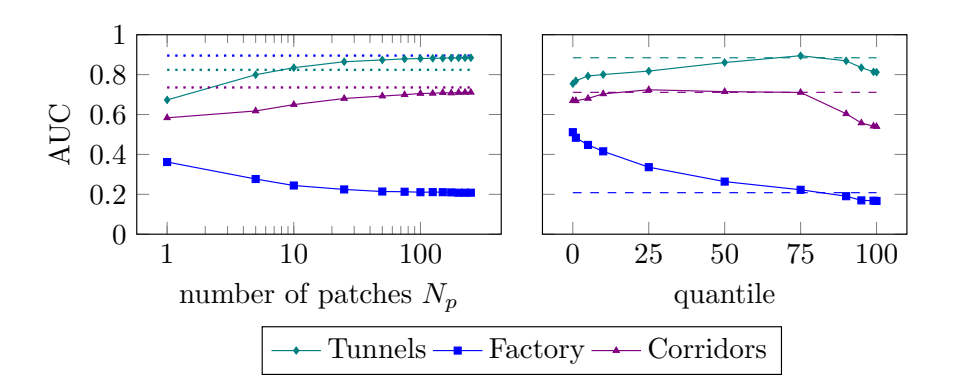


Figure 6: Results for model  $S_2$  when aggregating the scores of multiple patches extracted from each frame. Left: AUC, when aggregating by averaging, for different numbers of patches, compared to  $S_8$  (dotted). Right: AUC, when aggregating 250 patches by computing a quantile (solid) or by averaging (dashed).

## 5.3 Scales and anomalies

Table 1 summarizes the most important results on all model scales, datasets, and anomalies. We note that most anomalies are best detected by the full-frame approach  $S_8$ ; this is especially true for large-scale anomalies that cover a significant portion of the frame, such as smoke for Factory, or human and floor for Corridors. In contrast,  $S_8$  underperforms for small-scale anomalies, that cover few pixels of the downsampled image (e.g., dust and roots for Tunnels; cellophane, water, and hanging cable for Corridors); in this case, small-scale models sometimes have an advantage over  $S_8$ .

In contrast, we observe that small-scale models struggle with the large-scale smoke anomaly, returning consistently lower anomaly scores than normal frames, which yields AUC values well below 0.5. Figure 7 compares how  $S_1$ 

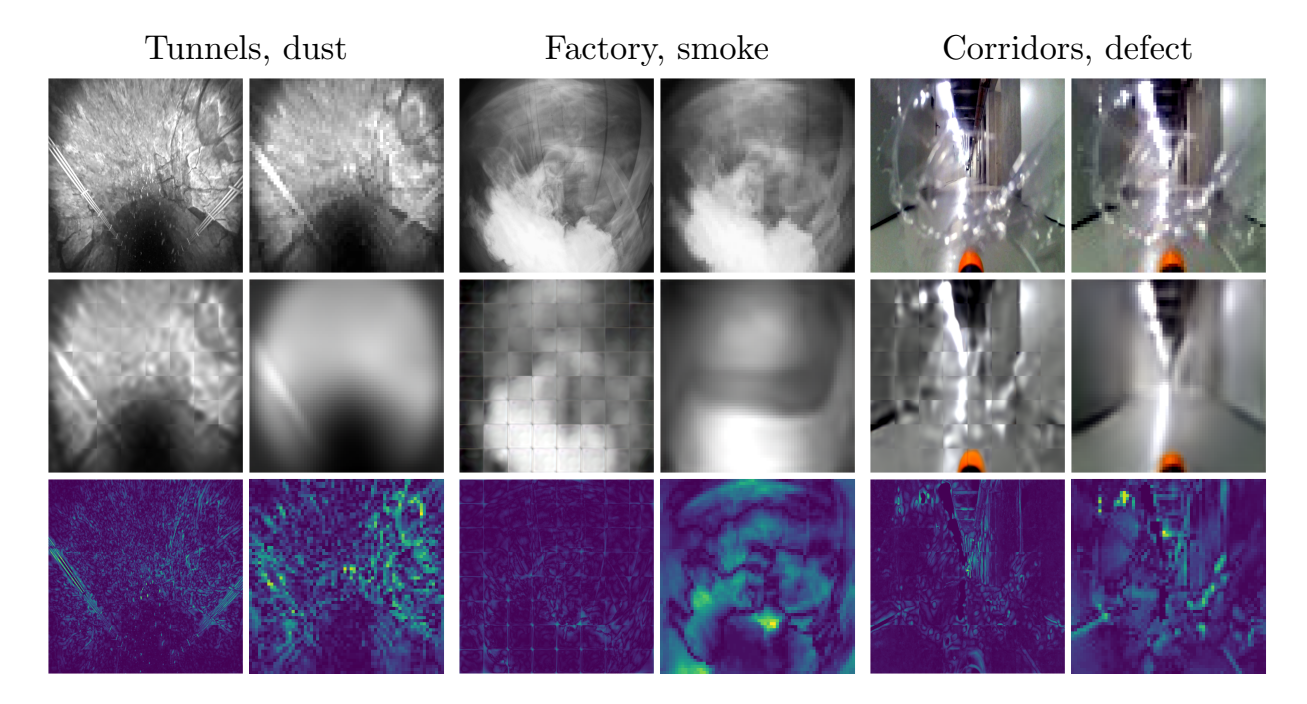


Figure 7: Comparison between  $S_1$  and  $S_8$ : pairs of identical input images representing an anomaly (top row); Autoencoder's outputs (central row) for  $S_1$  (left) and  $S_8$  (right); absolute value of the difference between input and output (bottom row, using a colormap where yellow is high and blue is low). Only for this illustration, for  $S_1$  we regularly sample 64 patches to cover the whole input image, and we use the output patches to compose a full-resolution image.

and  $S_8$  reconstruct a smoke frame: clearly,  $S_8$  fails to capture the large-scale structure of smoke, which yields high reconstruction error as expected in an anomalous frame; in contrast, since individual high-resolution patches of the smoke frame are low-contrast and thus easy to reconstruct, the  $S_1$  model yields very low reconstruction error and, thus, low AUC.

Some anomalies, such as *defect* for Corridors, are obvious enough that model at all scales can detect them almost perfectly.

#### 5.4 Run-time evaluation

The accompanying video features several runs where a quadcopter uses the  $S_8$  model to detects anomalies on-board to recognize and avoid unforeseen hazards. Figure 8 illustrates execution on a sequence that is part of the qualitative testing set for Factory; in the figure, we manually annotated the ground truth presence of hazards such as smoke (first red interval) and tape (second red interval). In the experiment, the robot captures a camera frame, computes an anomaly score and rises an alarm when the score passes a predefined threshold. The example shows how the drone is able to detect first a long area of smoke and later a small signaling tape.

## 6 Conclusions

We introduced three datasets for validating approaches to detect anomalies in visual sensing data acquired by mobile robots exploring an environment; various anomalies are represented, spanning from camera malfunctions to environmental hazards: some affect the acquired image globally; others only impact a small portion of it. We used these datasets to benchmark an anomaly detection approach based on autoencoders operating at different scales on the input frames. Results show that the approach is successful at detecting most anomalies (detection performance with an average AUC metric of 0.82); detecting small anomalies is in general harder than detecting anomalies that affect the whole image.

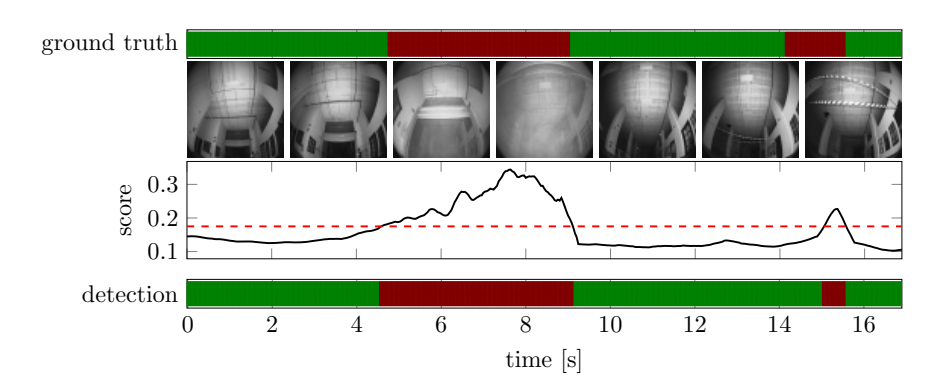


Figure 8: Part of the qualitative testing dataset in the Factory scenario where the drone first passes through smoke and then below a tape. Top: the manually added labels (green: normal, red: anomalous) and seven frames sampled from the timeline. Center: the score returned by the  $S_8$  model (solid black) and anomaly threshold t (dashed red). Bottom: the anomaly detector output.

# References

- [1] David Sloan Wilson, Anne B Clark, Kristine Coleman, and Ted Dearstyne. Shyness and boldness in humans and other animals. *Trends in ecology & evolution*, 9(11):442–446, 1994.
- [2] Lucia Moretti, Marleen Hentrup, Kurt Kotrschal, and Friederike Range. The influence of relationships on neophobia and exploration in wolves and dogs. *Animal Behaviour*, 107:159–173, 2015.
- [3] Mareike Stöwe, Thomas Bugnyar, Bernd Heinrich, and Kurt Kotrschal. Effects of group size on approach to novel objects in ravens (corvus corax). *Ethology*, 112(11):1079–1088, 2006.
- [4] Lorenz Wellhausen, René Ranftl, and Marco Hutter. Safe robot navigation via multi-modal anomaly detection. *IEEE Robotics and Automation Letters*, 5(2):1326–1333, 2020.
- [5] Matthew D Mitchell, Douglas P Chivers, Grant E Brown, and Maud CO Ferrari. Living on the edge: how does environmental risk affect the behavioural and cognitive ecology of prey? *Animal Behaviour*, 115:185–192, 2016.
- [6] Lukas Ruff, Jacob R Kauffmann, Robert A Vandermeulen, Grégoire Montavon, Wojciech Samek, Marius Kloft, Thomas G Dietterich, and Klaus-Robert Müller. A unifying review of deep and shallow anomaly detection. *Proceedings of the IEEE*, 2021.
- [7] Varun Chandola, Arindam Banerjee, and Vipin Kumar. Anomaly detection: A survey. *ACM computing surveys* (*CSUR*), 41(3):1–58, 2009.
- [8] Thomas Schlegl, Philipp Seeböck, Sebastian M Waldstein, Ursula Schmidt-Erfurth, and Georg Langs. Unsupervised anomaly detection with generative adversarial networks to guide marker discovery. In *International conference on information processing in medical imaging*, pages 146–157. Springer, 2017.
- [9] Luke Scime and Jack Beuth. A multi-scale convolutional neural network for autonomous anomaly detection and classification in a laser powder bed fusion additive manufacturing process. *Additive Manufacturing*, 24:273–286, 2018.
- [10] Matthias Haselmann, Dieter P Gruber, and Paul Tabatabai. Anomaly detection using deep learning based image completion. In 2018 17th IEEE International Conference on Machine Learning and Applications (ICMLA), pages 1237–1242. IEEE, 2018.
- [11] Punarjay Chakravarty, Alan M Zhang, Ray Jarvis, and Lindsay Kleeman. Anomaly detection and tracking for a patrolling robot. In *Australasian Conference on Robotics and Automation (ACRA)*. Citeseer, 2007.
- [12] Eliahu Khalastchi, Meir Kalech, Gal A Kaminka, and Raz Lin. Online data-driven anomaly detection in autonomous robots. *Knowledge and Information Systems*, 43(3):657–688, 2015.
- [13] Zachary Birnbaum, Andrey Dolgikh, Victor Skormin, Edward O'Brien, Daniel Muller, and Christina Stracquodaine. Unmanned aerial vehicle security using behavioral profiling. In 2015 International Conference on Unmanned Aircraft Systems (ICUAS), pages 1310–1319. IEEE, 2015.
- [14] Peter Christiansen, Lars N Nielsen, Kim A Steen, Rasmus N Jørgensen, and Henrik Karstoft. Deepanomaly: Combining background subtraction and deep learning for detecting obstacles and anomalies in an agricultural field. *Sensors*, 16(11):1904, 2016.

- [15] Mark A Kramer. Autoassociative neural networks. Computers & chemical engineering, 16(4):313–328, 1992.
- [16] Diederik P Kingma and Max Welling. Auto-encoding variational bayes. arXiv preprint arXiv:1312.6114, 2013.
- [17] Ian Goodfellow, Jean Pouget-Abadie, Mehdi Mirza, Bing Xu, David Warde-Farley, Sherjil Ozair, Aaron Courville, and Yoshua Bengio. Generative adversarial nets. *Advances in neural information processing systems*, 27, 2014.
- [18] Laurent Dinh, Jascha Sohl-Dickstein, and Samy Bengio. Density estimation using real nvp. *arXiv preprint* arXiv:1605.08803, 2016.
- [19] Ivan Kobyzev, Simon Prince, and Marcus Brubaker. Normalizing flows: An introduction and review of current methods. *IEEE Transactions on Pattern Analysis and Machine Intelligence*, 2020.
- [20] Lukas Ruff, Robert Vandermeulen, Nico Goernitz, Lucas Deecke, Shoaib Ahmed Siddiqui, Alexander Binder, Emmanuel Müller, and Marius Kloft. Deep one-class classification. In *International conference on machine learning*, pages 4393–4402. PMLR, 2018.
- [21] Sarah M Erfani, Sutharshan Rajasegarar, Shanika Karunasekera, and Christopher Leckie. High-dimensional and large-scale anomaly detection using a linear one-class svm with deep learning. *Pattern Recognition*, 58:121–134, 2016.
- [22] Mohammad Sabokrou, Mohammad Khalooei, Mahmood Fathy, and Ehsan Adeli. Adversarially learned one-class classifier for novelty detection. In *Proceedings of the IEEE Conference on Computer Vision and Pattern Recognition*, pages 3379–3388, 2018.
- [23] Natasa Sarafijanovic-Djukic and Jesse Davis. Fast distance-based anomaly detection in images using an inception-like autoencoder. In *International Conference on Discovery Science*, pages 493–508. Springer, 2019.
- [24] Christian Szegedy, Wei Liu, Yangqing Jia, Pierre Sermanet, Scott Reed, Dragomir Anguelov, Dumitru Erhan, Vincent Vanhoucke, and Andrew Rabinovich. Going deeper with convolutions. In *Proceedings of the IEEE conference on computer vision and pattern recognition*, pages 1–9, 2015.
- [25] Li Deng. The mnist database of handwritten digit images for machine learning research [best of the web]. *IEEE Signal Processing Magazine*, 29(6):141–142, 2012.
- [26] Han Xiao, Kashif Rasul, and Roland Vollgraf. Fashion-mnist: a novel image dataset for benchmarking machine learning algorithms. *arXiv preprint arXiv:1708.07747*, 2017.
- [27] A Krizhevsky. Learning multiple layers of features from tiny images. *Master's thesis, University of Tront*, 2009.
- [28] Eliahu Khalastchi, Gal A Kaminka, Meir Kalech, and Raz Lin. Online anomaly detection in unmanned vehicles. In *The 10th International Conference on Autonomous Agents and Multiagent Systems-Volume 1*, pages 115–122. Citeseer, 2011.
- [29] Mayu Sakurada and Takehisa Yairi. Anomaly detection using autoencoders with nonlinear dimensionality reduction. In *Proceedings of the MLSDA 2014 2nd workshop on machine learning for sensory data analysis*, pages 4–11, 2014.
- [30] Daehyung Park, Zackory Erickson, Tapomayukh Bhattacharjee, and Charles C Kemp. Multimodal execution monitoring for anomaly detection during robot manipulation. In 2016 IEEE International Conference on Robotics and Automation (ICRA), pages 407–414. IEEE, 2016.
- [31] Daehyung Park, Yuuna Hoshi, and Charles C Kemp. A multimodal anomaly detector for robot-assisted feeding using an lstm-based variational autoencoder. *IEEE Robotics and Automation Letters*, 3(3):1544–1551, 2018.
- [32] Alex Krizhevsky, Ilya Sutskever, and Geoffrey E Hinton. Imagenet classification with deep convolutional neural networks. *Advances in neural information processing systems*, 25:1097–1105, 2012.
- [33] Marco Hutter, Christian Gehring, Dominic Jud, Andreas Lauber, C Dario Bellicoso, Vassilios Tsounis, Jemin Hwangbo, Karen Bodie, Peter Fankhauser, Michael Bloesch, et al. Anymal-a highly mobile and dynamic quadrupedal robot. In 2016 IEEE/RSJ international conference on intelligent robots and systems (IROS), pages 38–44. IEEE, 2016.
- [34] Hannah R Kerner, Danika F Wellington, Kiri L Wagstaff, James F Bell, Chiman Kwan, and Heni Ben Amor. Novelty detection for multispectral images with application to planetary exploration. In *Proceedings of the AAAI Conference on Artificial Intelligence*, volume 33, pages 9484–9491, 2019.
- [35] Diederik P Kingma and Jimmy Ba. Adam: A method for stochastic optimization. arXiv preprint arXiv:1412.6980, 2014.